Supporting Information For

Intercalation-Enabled Reversible Disorder and Efficient Iodine Capture in a Two-Dimensional Metal–Organic Frameworks

Ruize Xie, Haoqing Jia, Peng Ye, Yin Chen*

College Chemistry & Chemical Engineering, Central South University, Changsha 410083, Hunan, China;

E-mail: chenyin@csu.edu.cn;

Table of Contents

A. General Remarks

Reagents and materials

I_2(AR), Cyanuric chloride (AR), Phloroglucinol (AR), N,N-Dimethylformamide (AR), Toluene (AR), K_2CO_3 (AR), $AlCl_3$ (AR), CrO_3 (AR), H_5IO_6 (AR) and $Cd(ClO_4)_2 \cdot 4H_2O$ were purchased from Aladdine chemical Co., Ltd. or Energy chemical Co., Ltd. All the chemicals were used without further purification.

Structural Characterization

The powder XRD results were recorded on a Rigaku ULTIMA IV X-ray powder diffractometer (XRD) with Cu Kα radiation (λ=1.5406 Å), 2-theta was run from 3° to 50° with a scan speed of 2°/min. Thermogravimetric analyses (TGA) were carried out on a NETZSCH STA 449 F3 model with thermal analyzer heating from room temperature to 600 °C at the rate of 5 °C·min $^{-1}$ in nitrogen. Infrared spectra (transmission) were recorded on a Nicolet Magna 6700 FT spectrometer. Raman spectra were recorded on a Horiba LabRAM HR Evolution model. Scanning electron microscopy (SEM) images were taken on JEOL/JSM-7610Fplus (100KV), equipped with a super EDX (EDS model). X-ray photoemission spectroscopy experiments (XPS) were performed in the Thermo Scientific K-Alpha+ XPS System. The XPS spectrum was recorded using monochromatic Al Ka X-ray source (1486.6 eV) operating at 72 W with a base pressure of 6.8×10^{-9} Torr. Survey spectrum and high-resolution spectrum were recorded with a pass energy of 150 eV and 50 eV，respectively. The XPS data were calibrated by using adventitious C 1s signal at 284.8 eV as reference and the binding energy spectra were fitted by Avantage software, Shirley background was used for all spectra.

B. Experimental Details

Methods

Preparation of IPM-1: Bicyclocalix[2]arene[2]triazines tricarboxylic acid (BCTA, 250 mg, 0.30 mmol) and $MnCl_2 \cdot 4H_2O$ (495 mg, 2.50 mmol) were dissolved in dimethylformamide (DMF, 50 mL) in a Schlenk tube. The mixture was sealed and heated at 120 °C for 48 h under static conditions. After naturally cooling to room temperature, colorless block-shaped crystals were obtained. The crystals were collected by filtration and washed with fresh DMF twice to afford **IPM-1** as a crystalline solid.

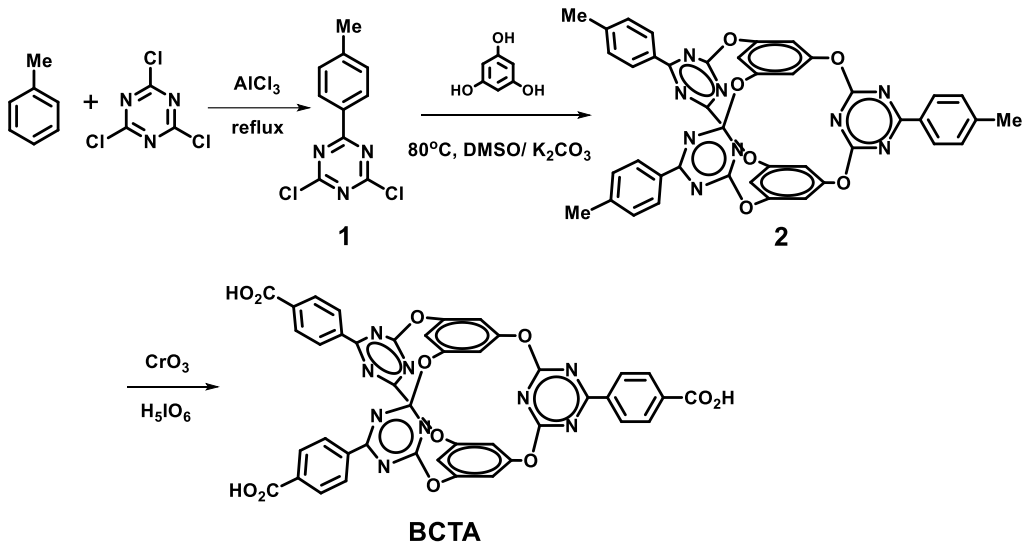

Scheme S1: The synthesis of **BCTA**.

Synthesis of BCTA: BCTA was synthesized via the synthetic route as shown in scheme S1.

CrO_3 (120 mg, 1.20 mmol) and H_5IO_6 (320 mg, 1.40 mmol) were added to acetonitrile (40 mL) in a 100 mL single-neck round-bottom flask and stirred until complete dissolution. A solution of compound **2** (0.30 g, 0.40 mmol) in acetonitrile/dichloromethane (1:1, v/v; 10 mL) was then added dropwise over 15 min, during which a yellow precipitate gradually formed. The reaction mixture was further stirred for 10 h at room temperature, followed by solvent removal under reduced pressure. The residue was washed with deionized water and extracted with ethyl acetate. The organic phase was dried over anhydrous Na_2SO_4 and concentrated to afford an off-

white crude product (0.29 g, 90% yield). Recrystallization from a mixed solvent of tetrahydrofuran and acetonitrile afforded crystalline **BCTA** (0.30 g, 89% yield).

Iodine Vapor Adsorption

A known mass of **IPM-1** was placed in a 20 mL glass vial and weighed accurately. The vial was then placed inside a larger sealed glass container (100 mL) containing excess solid iodine. The sealed system was heated at 80 °C in a forced-air oven to promote iodine sublimation and adsorption.

During the adsorption process, the color of IPM-1 gradually changed from white to dark black. At predetermined time intervals, the sample vial was removed and weighed until no further mass increase was observed, indicating adsorption equilibrium. The iodine uptake capacity (Q, $g \cdot g^{-1}$) was calculated using the following equation:

$$Q = \frac{m_1 - m_2}{m_1}$$

where m_1 and m_2 are the masses of **IPM-1** before and after iodine adsorption, respectively.

IPM-1 reached adsorption equilibrium within 10 h, with a saturated iodine uptake capacity of 1.85 $g \cdot g^{-1}$. The adsorption kinetics were analyzed by linear fitting using pseudo-first-order and pseudo-second-order kinetic models. The experimental data exhibited a significantly better fit to the pseudo-second-order model ($R^2 > 0.998$), indicating that the adsorption process is governed by chemisorption-related kinetics.

The retention stability of iodine-loaded **IPM-1** (denoted as **IPM-1@I_2**) was evaluated by monitoring the residual mass over time. The iodine content remained essentially unchanged over 7 days under ambient conditions, demonstrating the stable and persistent iodine-capturing capability of **IPM-1**.

Iodine Adsorption from Liquid Phase

A cyclohexane solution of iodine (1 $g \cdot L^{-1}$) was prepared in a glass vial, and its initial absorbance (C_0) was recorded using UV–vis spectroscopy. A known amount of

IPM-1 crystals was then added to the solution. At specified time intervals, aliquots of the solution were withdrawn, filtered through a 0.22 μm membrane, and their absorbance values (C′) were measured.

The equilibrium adsorption capacity (Q_e) was calculated using the following equation:

$$Q_e = \frac{(C_o - C_e) * V}{m}$$

where V (L) is the volume of the iodine solution, m (g) is the mass of **IPM-1**, and C_o and C_e ($mg \cdot L^{-1}$) are the initial and equilibrium concentrations of iodine, respectively. Q_e ($mg \cdot g^{-1}$) represents the amount of iodine adsorbed per gram of adsorbent.

The iodine adsorption isotherms were fitted using the Langmuir model:

$$Q_e = \frac{Q_{max} K_L C_e}{1 + K_L C_e}$$

where Q_{max} ($mg \cdot g^{-1}$) is the maximum adsorption capacity and K_L is the Langmuir constant. The linear Langmuir fitting yielded a correlation coefficient (R^2) of 0.9986, while the nonlinear fitting gave an R^2 value of approximately 0.97, indicating that the Langmuir model adequately describes the iodine adsorption behavior of **IPM-1**. These results suggest a predominantly monolayer adsorption process with uniformly distributed adsorption sites and negligible intermolecular interactions among iodine molecules. Based on the Lambert–Beer law, the maximum adsorption capacity was determined to be 860 $mg \cdot g^{-1}$.

Co-crystallization of IPM-1 with Iodine

BCTA (25 mg, 0.03 mmol), $MnCl_2 \cdot 4H_2O$ (50 mg, 0.25 mmol), and iodine (10 mg) were dissolved in DMF (5 mL) in a Schlenk tube. The sealed tube was heated at 120 °C, resulting in the formation of yellow crystalline solids. The obtained crystals exhibited poor crystallinity and were unsuitable for single-crystal X-ray diffraction analysis. Preliminary diffraction data indicated lattice parameters comparable to those of pristine **IPM-1** (Table S2), suggesting that the presence of iodine does not alter the

overall crystal framework of **IPM-1** but induces pronounced structural disorder and reduced crystal quality.

Crystallographic Information File of IPM-1

The experimental X-ray single crystal data of **IPM-1** (CCDC2031603) can be accessed from Cambridge Crystallographic Data Centre and Fachinfor mationszentrum Karlsruhe Access Structures service: www.ccdc.cam.ac.uk/structures.

In the original crystallographic data from single crystal X-ray diffraction (SCXRD), accurate Miller index assignment for the plane of the **IPM-1** layer could not be achieved within the pristine lattice framework. Accordingly, unit cell transformation was performed on the solved SCXRD structure using Crystal Maker software: the unit cell of the known SCXRD structure was transformed to align the 2D layers within the ab-plane with stacking along the c-axis (Data S1), and the transformed unit cell contained the minimal repeating unit of one **IPM-1** layer, to facilitate the structural analysis and diffraction peak assignment of the powder X-ray diffraction (PXRD) pattern.

C. Crystal Structure and EDS Datasheet

Table S1. Crystal Structure and Refinement Datasheet

Compound	**IPM-1**
Empirical formula	$C_{87}H_{49}Mn_3N_{19}O_{28}$
Chemical structure	$Mn_3(BCTA)_2 \cdot DMF \cdot 3H_2O$
Formula weight	1973.27
Temperature	193(2) K
Wavelength	1.34139 Å
Crystal system	Triclinic
Space group	P-1
a [Å]	21.4111(17)
b [Å]	22.6255(17)
c [Å]	23.2304(17)
α [deg]	61.166(3)
β [deg]	64.616(3)
γ [deg]	74.946(4)
V[Å^3]	8886.7(12)
Z	2
ρ [g/cm3]	0.737
Absorption coefficient	1.429 mm-1
F(000)	2006
Crystal size [mm^3]	0.100 x 0.050 x 0.030
Theta range for data collection	1.944 to 52.999°.
Index ranges	-25<=h<=25, -26<=k<=26, -27<=l<=27
Reflections collected	408987
Independent reflections	31414 [R(int) = 0.1054]
Refinement method	Full-matrix least-squares on F2
Data / restraints / parameters	31414 / 1 / 1239
Goodness-of-fit	1.066
R1,wR2 [I>2σ(I)]	0.0772, 0.2480
R1,wR2 (all data)	0.0968, 0.2690
Largest diff. peak and hole	0.929 and -1.061 e.Å-3

Table S2: Fitting results are based on the Pseudo-first-order kinetic and Pseudo-second-order kinetic models

Kinetic model	Parameters
Pseudo-first-order	k_1= 0.00682 min^{-1}
	R^2=0.991
	q_e= 1689 $mg \cdot g^{-1}$
Pseudo-second-order	k_2= 5.3996*10^{-5} $g \cdot (mg \cdot min)^{-1}$
	R^2=0.999
	q_e= 1853 $mg \cdot g^{-1}$

Table S3. Summary of iodine adsorption in MOFs via vapor diffusion

MOF	BET surface area (m^2g^{-1})	Pore volume (cm^3g^{-1})	Iodine uptake ($g\ g^{-1}$)	Ref.
$[Cu_4I_4(L_3)]$	641	0.31	0.14	Chem. Commun., 52, 12702, (2016).
UPC-158	2170	0.93	1.78	J. Mater. Chem. A, **7**, 13173, (2019).
$Zn_2(TMTB)(H2O)_2]\cdot(OH^-)$	670	0.29	2.00	Cryst. Growth Des. 24, 5648, (2024).
PCN-333(Al)	2935	2.97	4.42	J. Mater. Chem. A, **7**, 18324, (2019).
$Fe_3(HCOO)_6$	385	0.15	0.49	Adv. Funct. Mater. 17, 1523, (2007).
MIL-53-SH(Al)	324	0.07	0.33	Cryst Eng Comm 18, 8108, (2016).
Cu-BTC	1850	0.74	1.75	Chem. Mater. 25, 2591, (2013).
MOF-867	2403	1.12	0.88	ACS Appl. Mater. Interfaces 12, 20429, (2020).
Co-tib	-	-	7.68	J. Am. Chem. Soc. 147, 32352, (2025).
$[Zn_3(OH)(H_2O)(IPDA)_2$ (HIPDA)·xsolvent]	-	-	4.86	Inorg. Chem. Front., 11, 769, (2024).
Th-UiO-66-$(NH_2)_2$	641	-	0.96	Chem. Eur. J., 27, 1286, (2021)
ZIF-8	1630	0.66	1.25	Cryst Eng Comm, 16, 8660, (2014)
MFM-300(Fe)	1192	0.46	1.29	J. Am. Chem. Soc., 139, 16289, (2017)
HKUST-1@PES	1250	-	0.376	Adv. Funct. Mater., 28, 1, (2018)
IPM-1	210	0.13	1.85	This work

Table S4: Summary of the compositions in IPM-1@I2 determined by EDS

Sample	Element	wt%	At%
Gas-phase	Mn	10.9	22.1
absorbed	I	89.1	77.9
IPM-1@I2	In total[a]	100.00	100.00
IPM-1@I2	Mn	75.3	87.7
Treated in	I	24.7	12.3
Ethanol	In total	100.00	100.00
Liquid-phase	Mn	54.2	73.2
absorbed	I	45.8	26.8
IPM-1@I2	In total	100.00	100.00

a. Owing to signal interference from the silicon substrate and inherent limitations in light element detection, Mn was used as the internal reference to semi-quantitatively evaluate the iodine loading of the sample via the I/Mn elemental ratio.

Table S5: Fitting results for the Langmuir model.

Isotherm model	Parameters
Langmuir	q_m= 945 mg·g^{-1}
	K_L= 0.008685 L·mg^{-1}
	R^2= 0.999

Table S6. Summary of iodine adsorption in MOFs via solution-based processes

MOF	Solution	BET surface area (m^2g^{-1})	Pore volume (cm^3g^{-1})	Iodine uptake (g g^{-1})	Ref.
$[Cd(bdc)(4\text{-}bpmh)]_n$	Hexane	36	0.09	0.15	Chem. Eur. J. 21, 9306, (2015).
Cu_2TMBD	Hexane	197	0.15	0.18	Inorg. Chem. 57, 4807, (2018).
MIL-53-NH2(Al)	Cyclohexane	735	0.35	0.18	Eur. J. Inorg. Chem. 713, (2021).
JLU-Liu31	Cyclohexane	1700	0.85	0.25	J. Mater. Chem. A 4, 15081, (2016).
UIO-66	Cyclohexane	1970	0.89	0.667	Dalton Trans. 46, 7412, (2017).
HKUST-1@PES	Cyclohexane	1250	-	0.376	Adv. Funct. Mater. 28, 1, (2018).
Th-UiO-66-$(NH_2)_2$	Cyclohexane	641	-	0.24	Chem. Eur. J., 27, 1286, (2021)
MIL-101-NH2(Al)	Cyclohexane	2100	1.12	0.31	Chem. Commun., 49, 10320, (2013)
IPM-1	Hexane	210	0.13	0.86	This work

Table S7. Cell parameters of co-crystal of IPM-1 with Iodine

Compound	**IPM-1 absorbed I_2**	**IPM-1 co-crystalized with I_2**	
Temperature	193(2) K	193(2) K	193(2) K
Wavelength	1.34139 Å	1.34139 Å	1.34139 Å
Crystal system	Triclinic	Triclinic	Triclinic
Space group	P-1	P-1	P-1
a [Å]	21.002(4)	21.184(3)	21.524(3)
b [Å]	22.356(0)	21.980(3)	22.100(3)
c [Å]	22.954 (5)	22.959 (3)	23.014 (3)
α [deg]	61.973(4)	77.826(5)	77.477(3)
β [deg]	63.109(3)	62.608(4)	62.360(5)
γ [deg]	77.163(0)	62.575(4)	62.115(4)
V[$Å^3$]	8484.1(1)	8424.6(18)	8571.2(12)
Z	1	1	1

D. Crystal Structure and other characterization figures

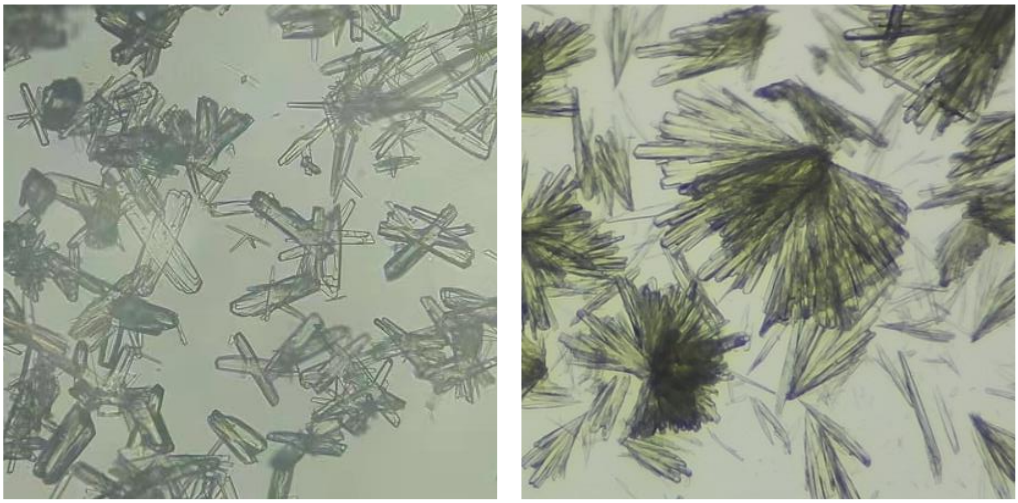

Fig. S1: The microphotography photos of fresh-prepared IPM-1 crystals, with regular crystal appearance and millimeter-scale size.

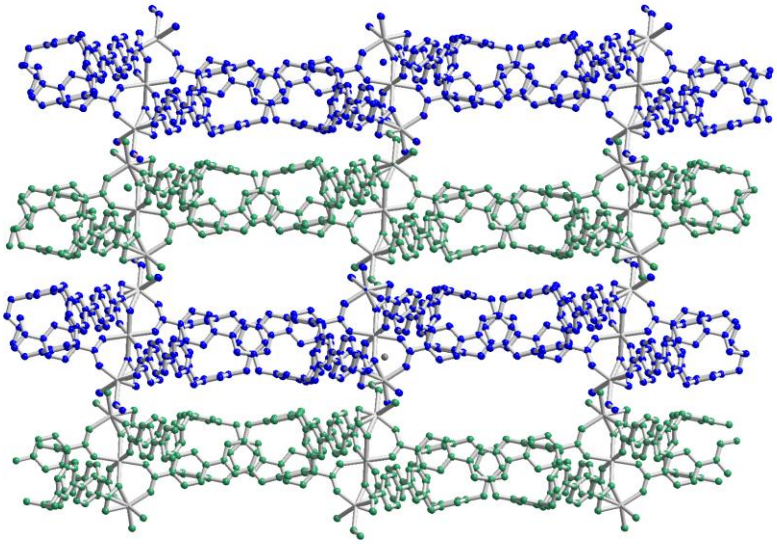

Fig. S2: The side view of ABAB stacking architecture of **IPM-1** lattice.

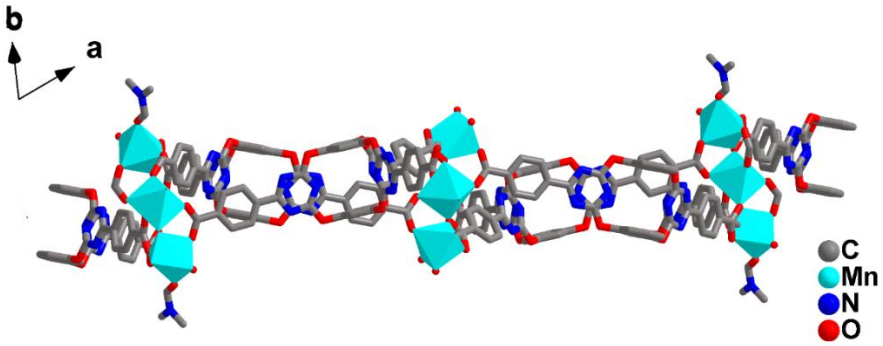

Fig. S3: The side view of one single **IPM-1** layer.

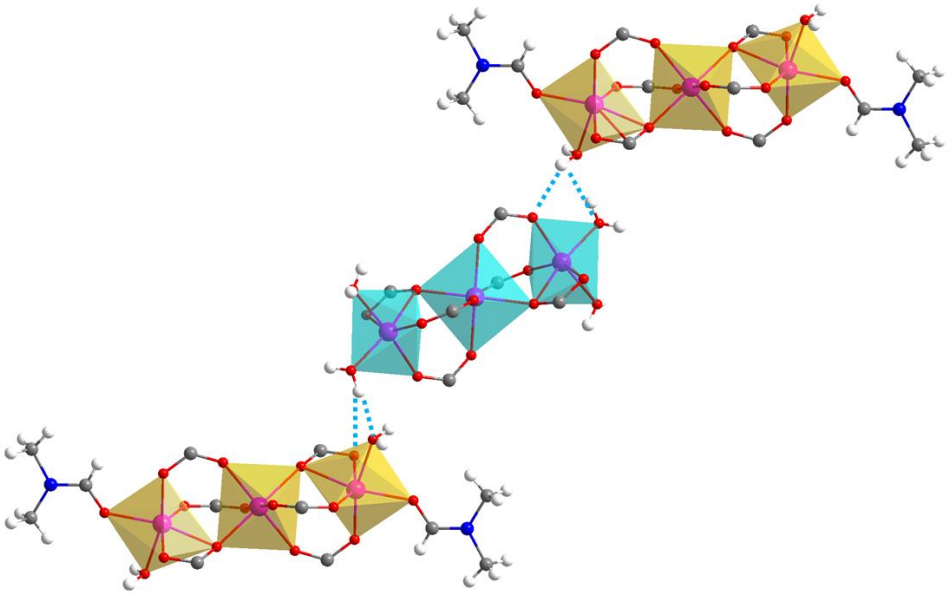

Fig. S4: The hydrogen bonding between the $[Mn_3(O_2C)_6]\bullet 4H_2O$ cluster and $[Mn_3(O_2C)_6]\bullet 2H_2O\bullet 2DMF$ cluster.

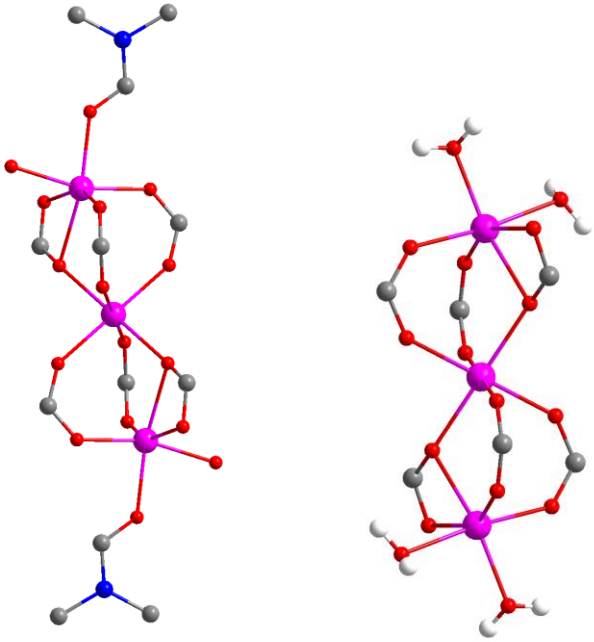

Fig. S5: The structure of $[Mn_3(O_2C)_6]\bullet 2H_2O\bullet 2DMF$ cluster (left) and $[Mn_3(O_2C)_6]\bullet 4H_2O$ cluster (right).

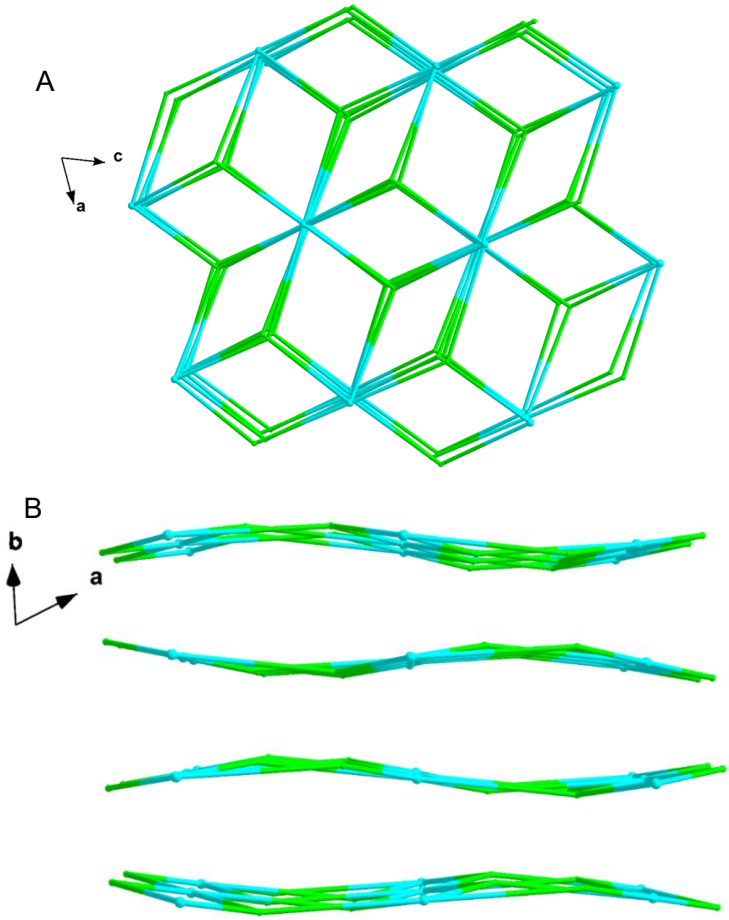

Fig. S6: (A) The top view of the three-dimensional framework with regular channels in **IPM-1.** (B) The ABAB stacking fashion with the 3,6-connected net nodes in **IPM-1**.

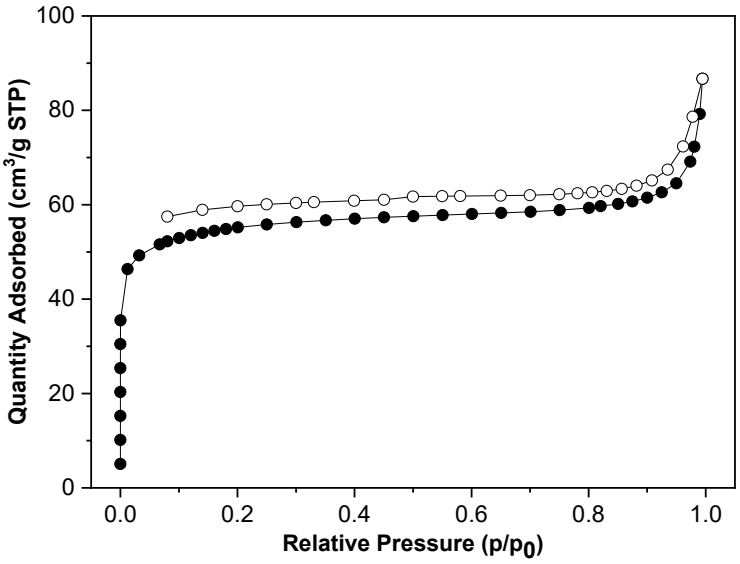

Fig. S7: N2 adsorption and desorption isotherms at 77K of **IPM-1** crystals, activated at 100 °C under vacuum for 8 h.

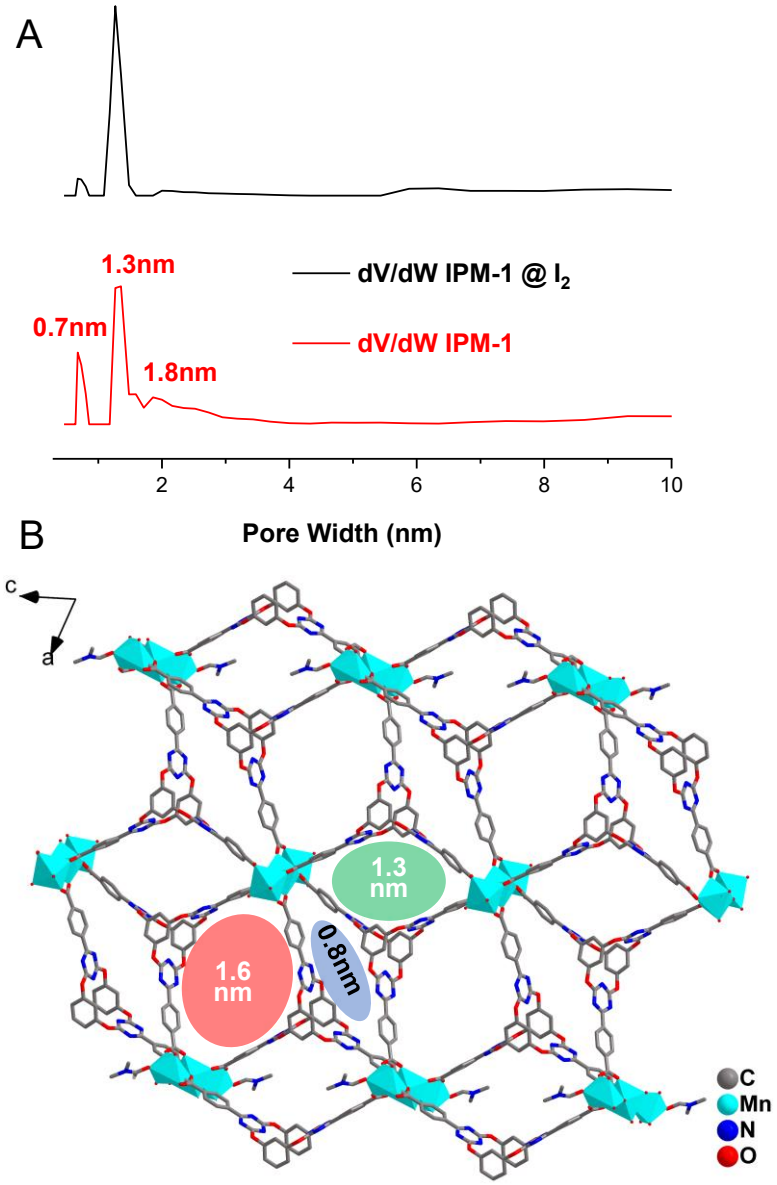

Fig. S8: (A) Narrow pore-size distribution of **IPM-1** and **IPM-1 @I2** after iodine desorption. (B) The representation of a single layer in IPM-1 and the three types of pores with different sizes.

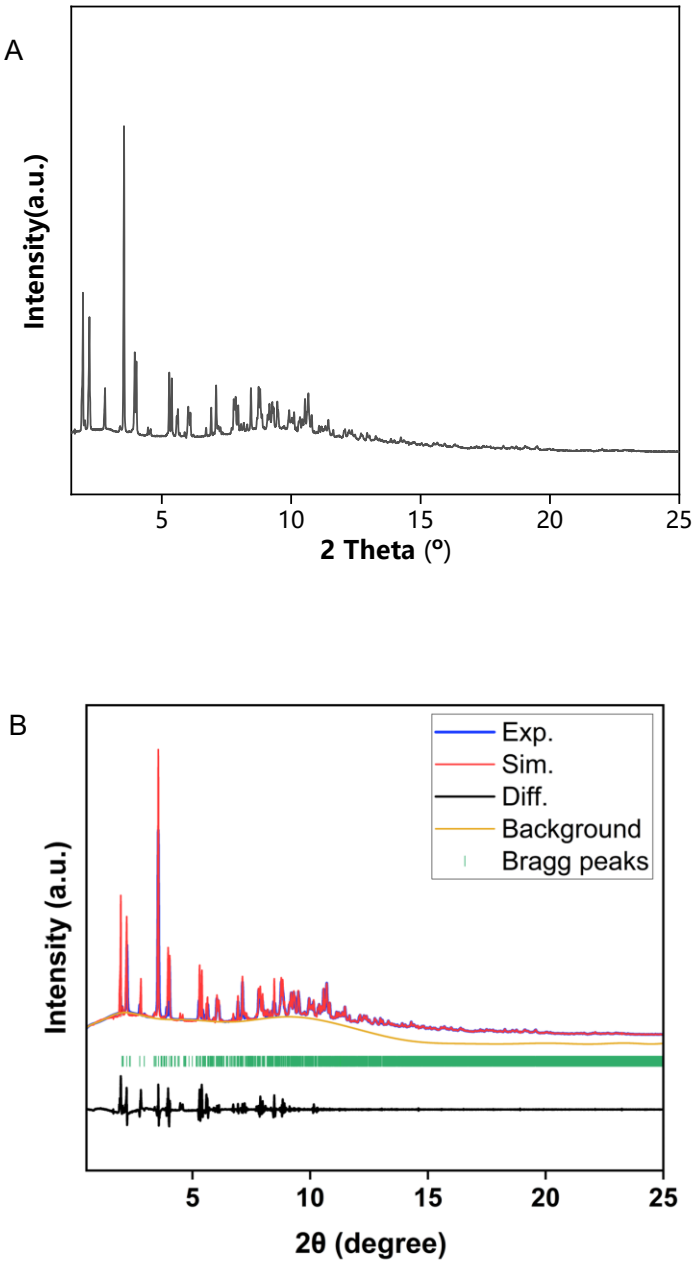

Fig. S9: (A) SR-PXRD pattern of **IPM-1**; (B) Rietveld refinement confirms that the experimental PXRD pattern is in good agreement with the theoretically simulated pattern.

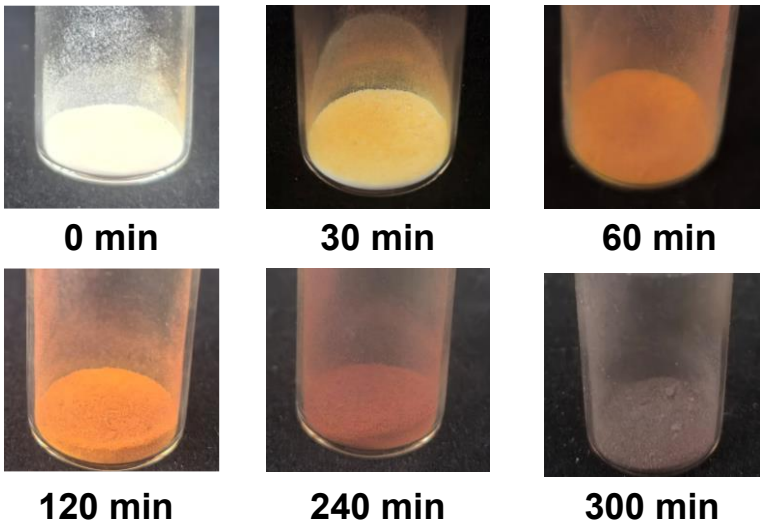

Fig. S10: Color changes of **IPM-1** crystals during iodine vapor adsorption at different time intervals.

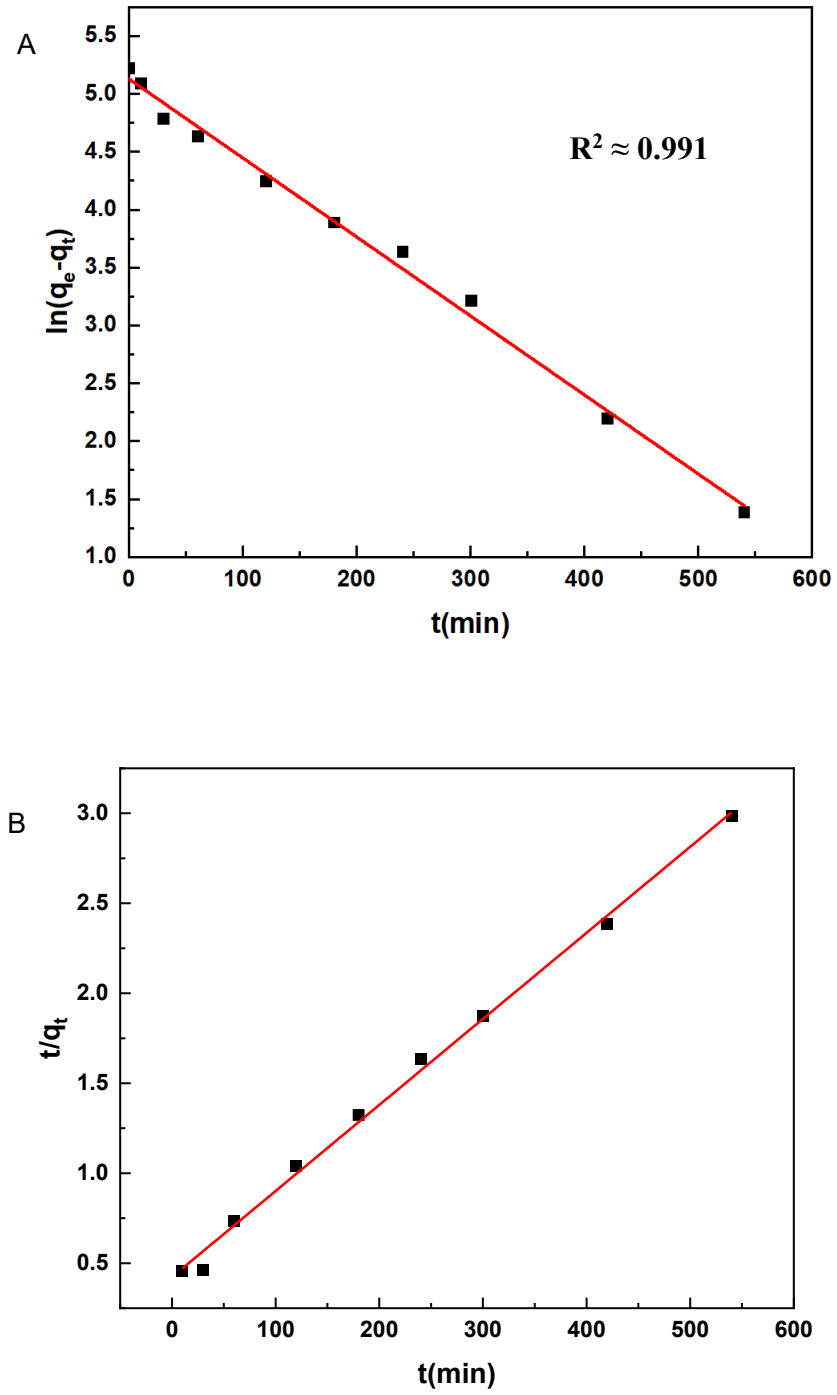

Fig. S11: Gas-phase iodine uptake–time profile of **IPM-1** fitted with first-order kinetic model (A) and second-order kinetic model (B).

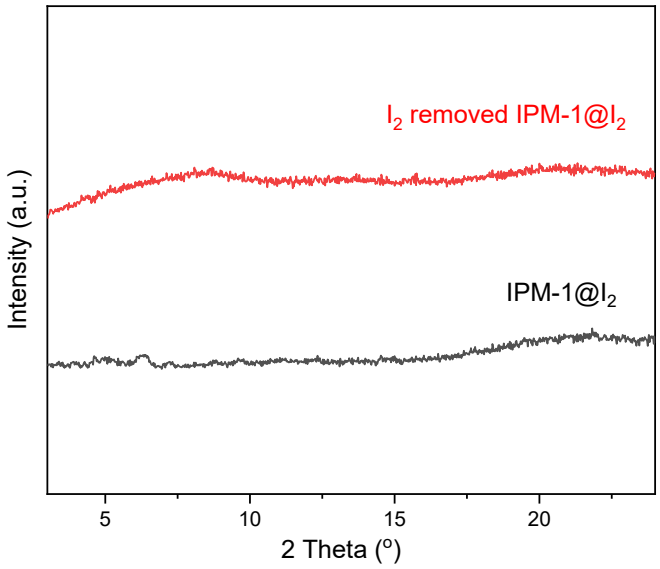

Fig. S12: Comparison of PXRD patterns of **IPM-1** with saturated iodine loading (black), and after treatment in DMF at 120 °C (red).

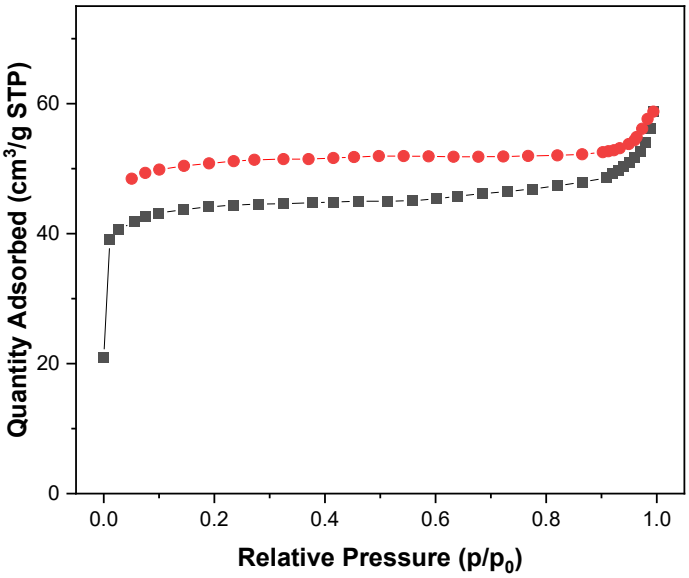

Fig. S13: N2 adsorption and desorption isotherms at 77K of **IPM-1@I2** after iodine desorption, activated at 100 °C under vacuum for 8 h.

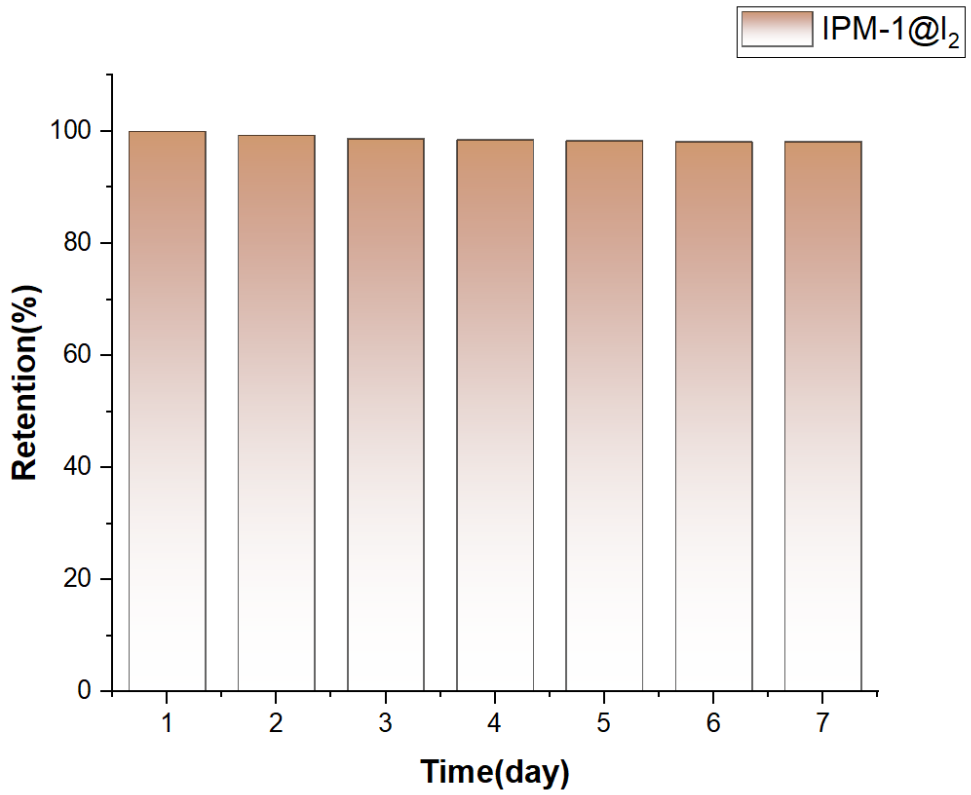

Fig. S14: The retention stability of **IPM-1** with saturated iodine loading.

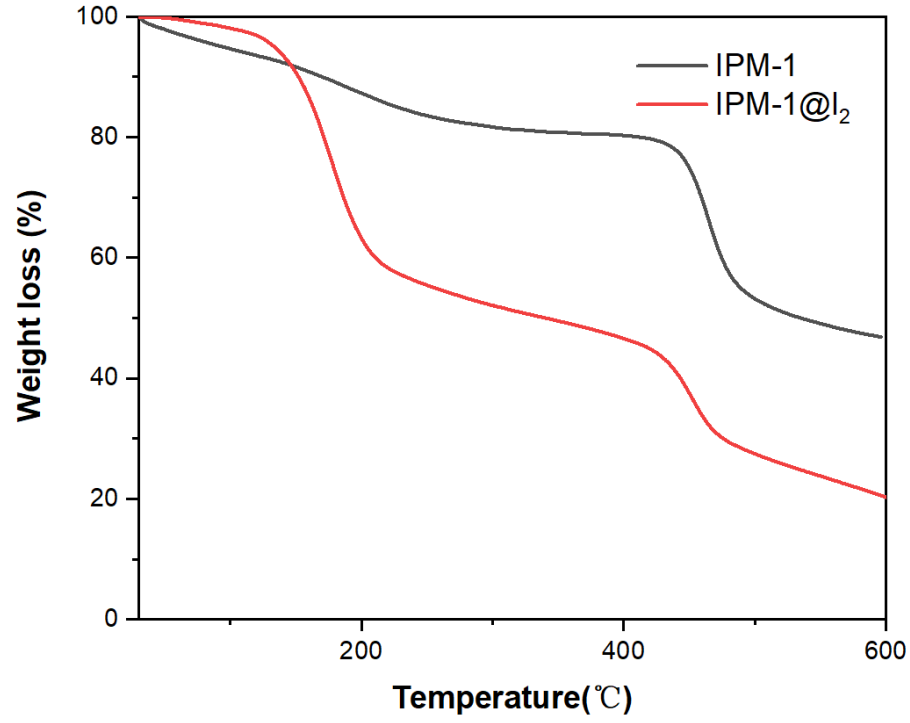

Fig. S15: Comparison of TGA curves of **IPM-1**with **IPM-1@I₂**.

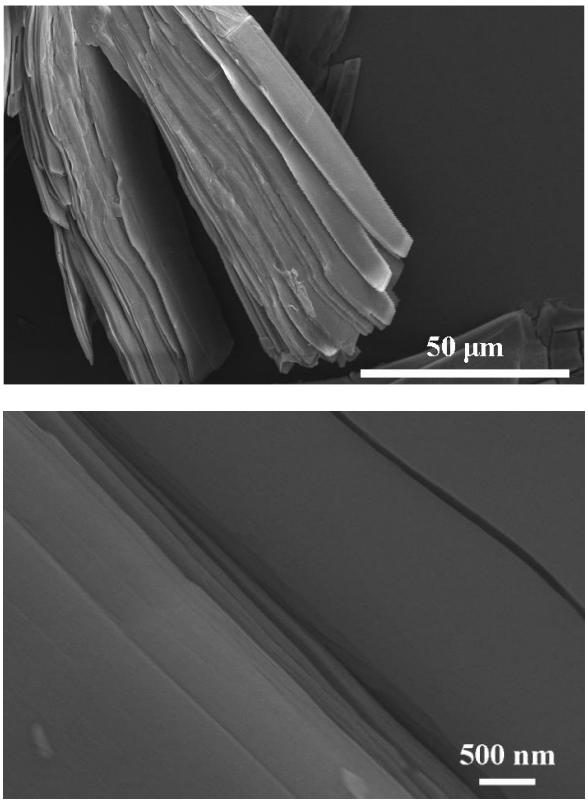

Fig. S16: SEM images of pristine **IPM-1** crystals.

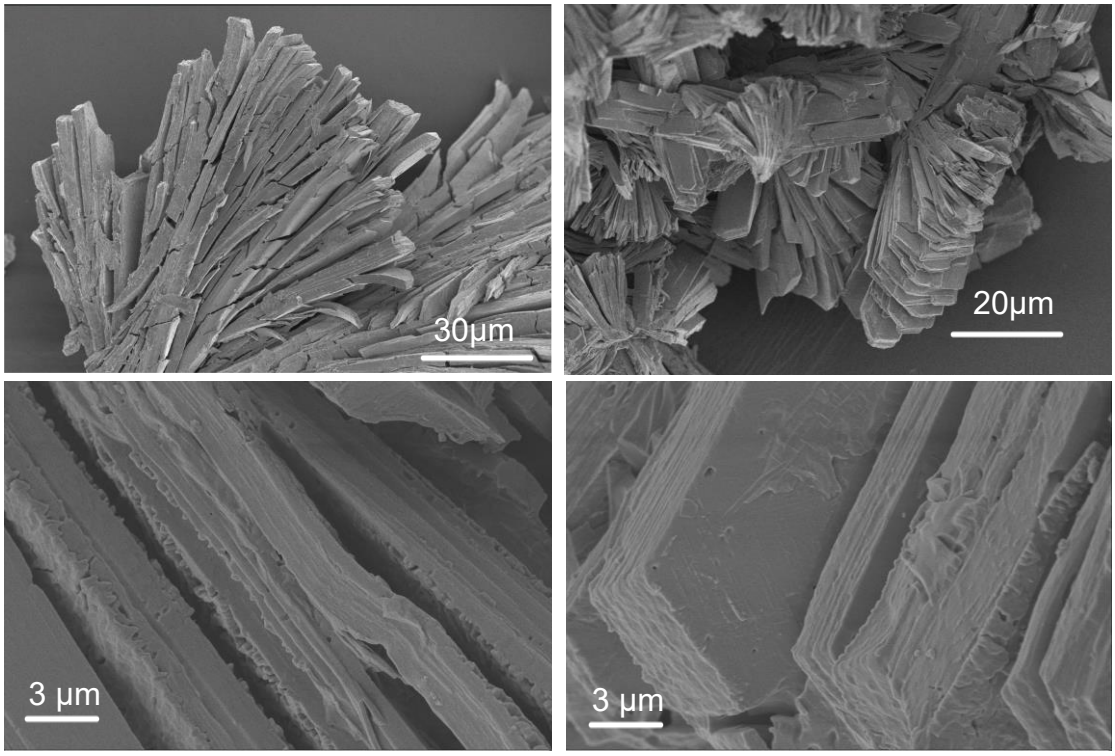

Fig. S17: SEM images of **IPM-1@I_2**.

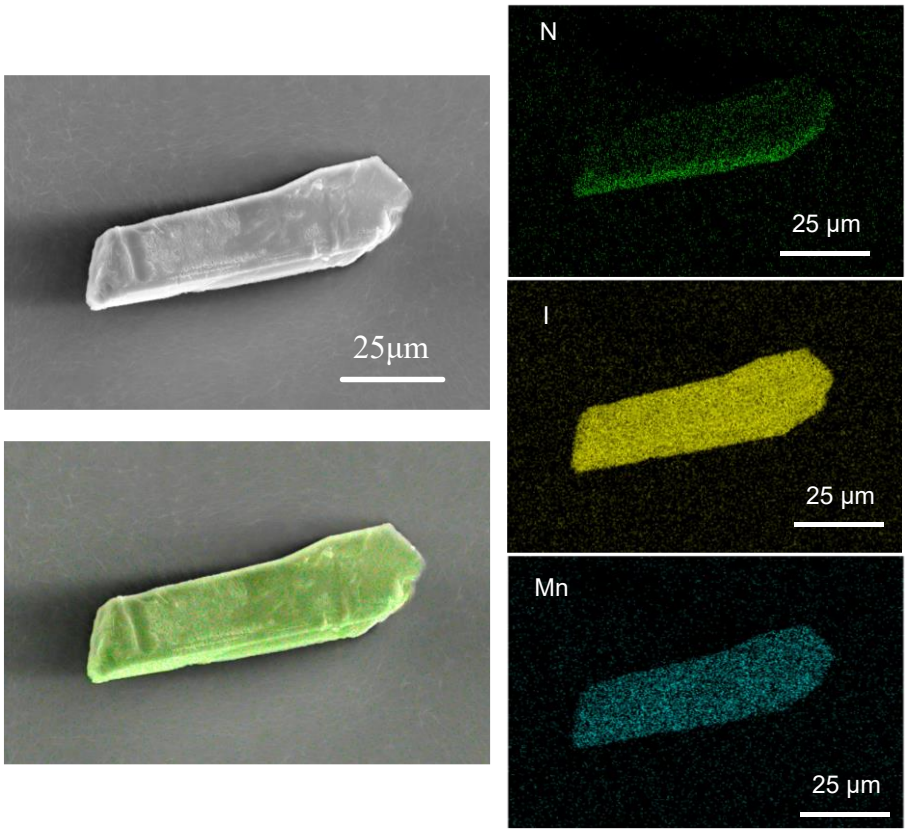

Fig. S18: EDS mapping image of **IPM-1** crystal grain with saturated iodine loading.

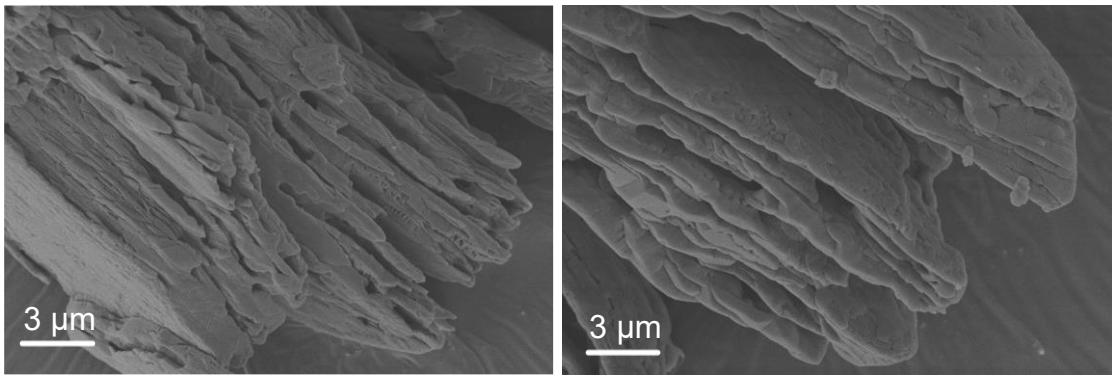

Fig. S19: SEM images of **IPM-1@I_2** after iodine desorption.

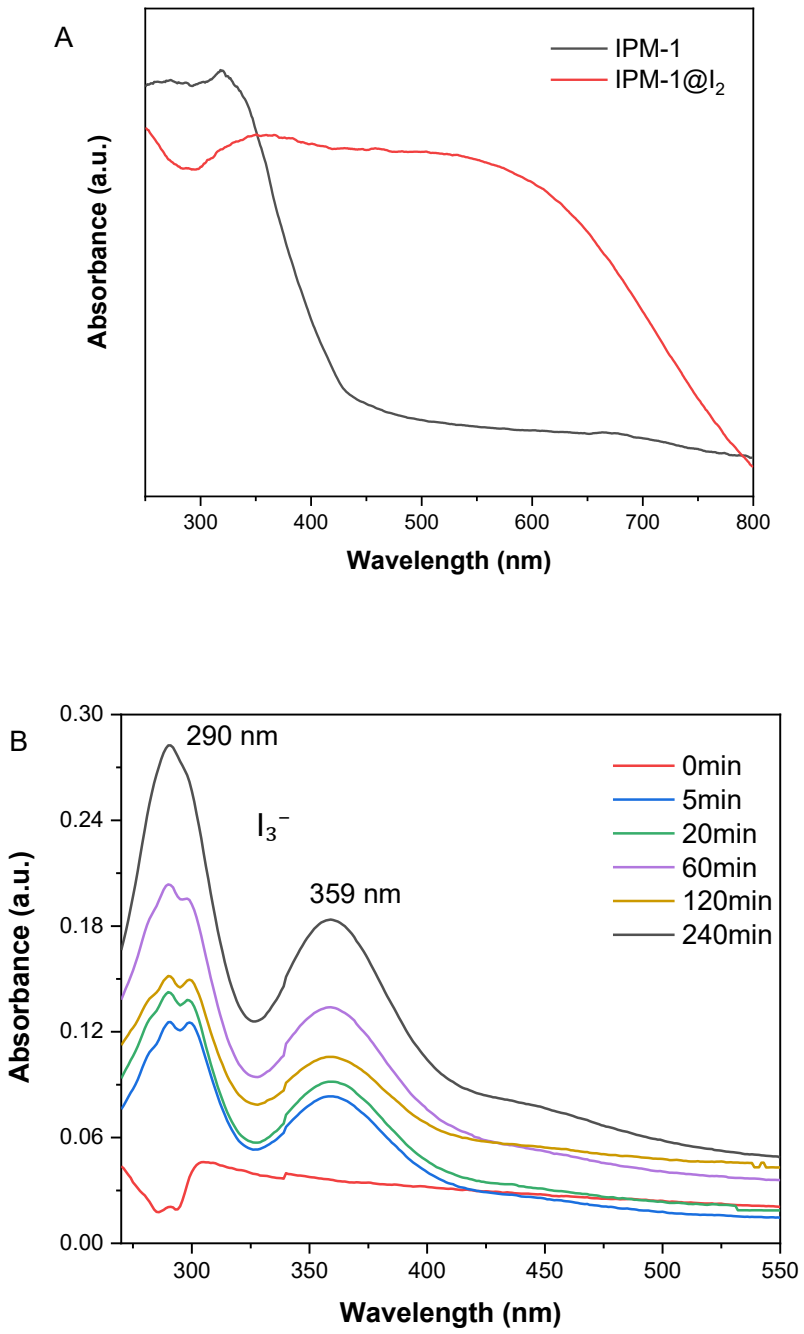

Fig. S20: (A) Comparison of the solid-state UV-Vis spectra of **IPM-1** and **IPM-1@I₂**; (B) UV-Vis spectra revealing the release of I_2 from **IPM-1@I₂** over time, showing the characteristic absorbance bands of I_3^-.

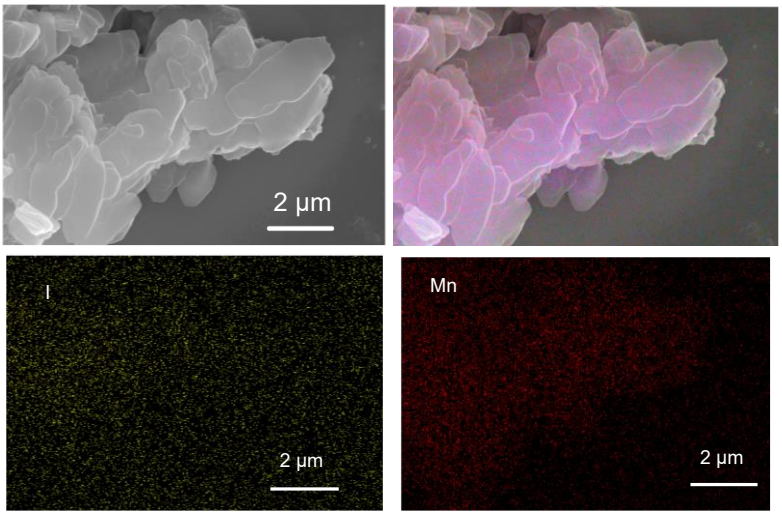

Fig. S21: EDS mapping images of **IPM-1@I_2** after immersed in ethanol.

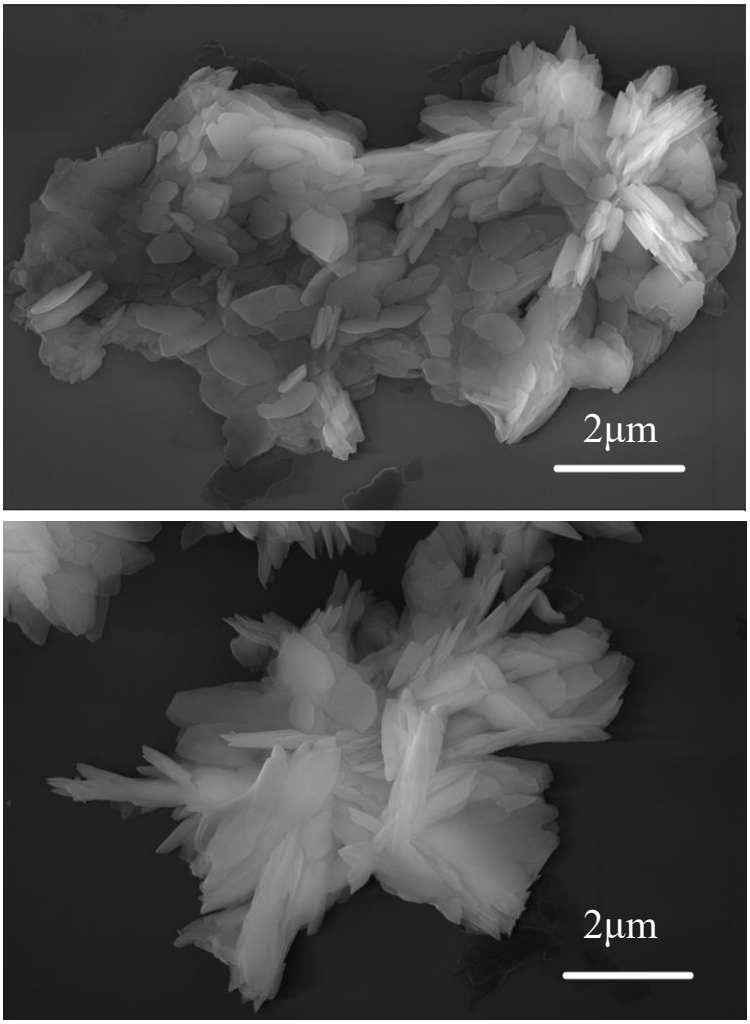

Fig. S22: SEM image of **IPM-1@I_2** after iodine desorption in ethanol.

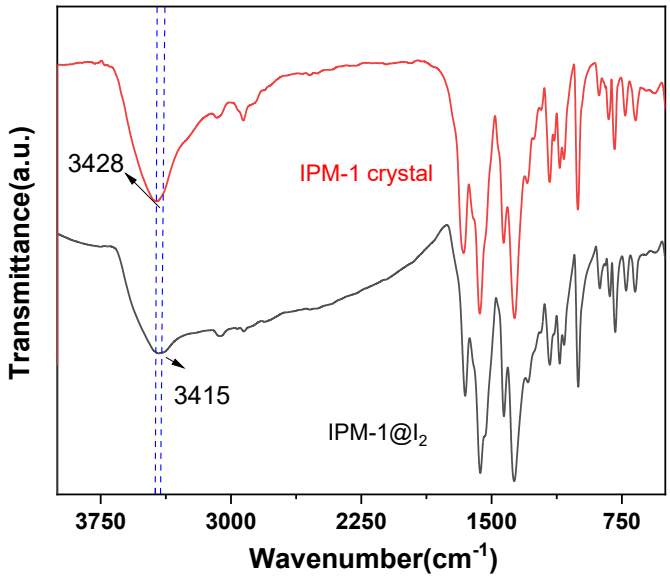

Fig. S23: Comparison of FT-IR spectra of pristine **IPM-1** and **IPM-1@I₂**, with noticeable changes primarily observed in the O–H stretching region.

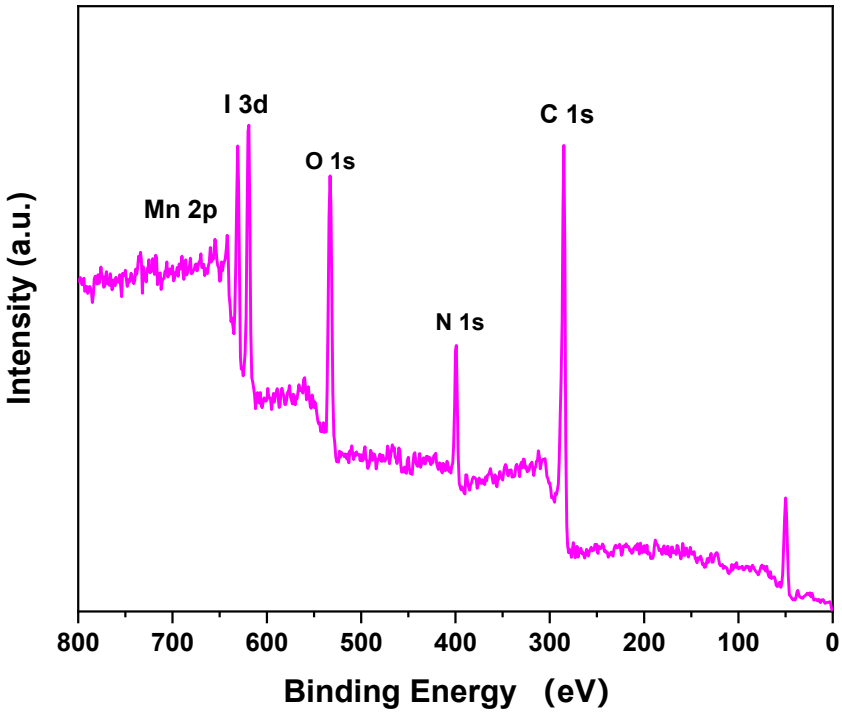

Fig. S24: XPS survey spectrum of **IPM-1@I₂**.

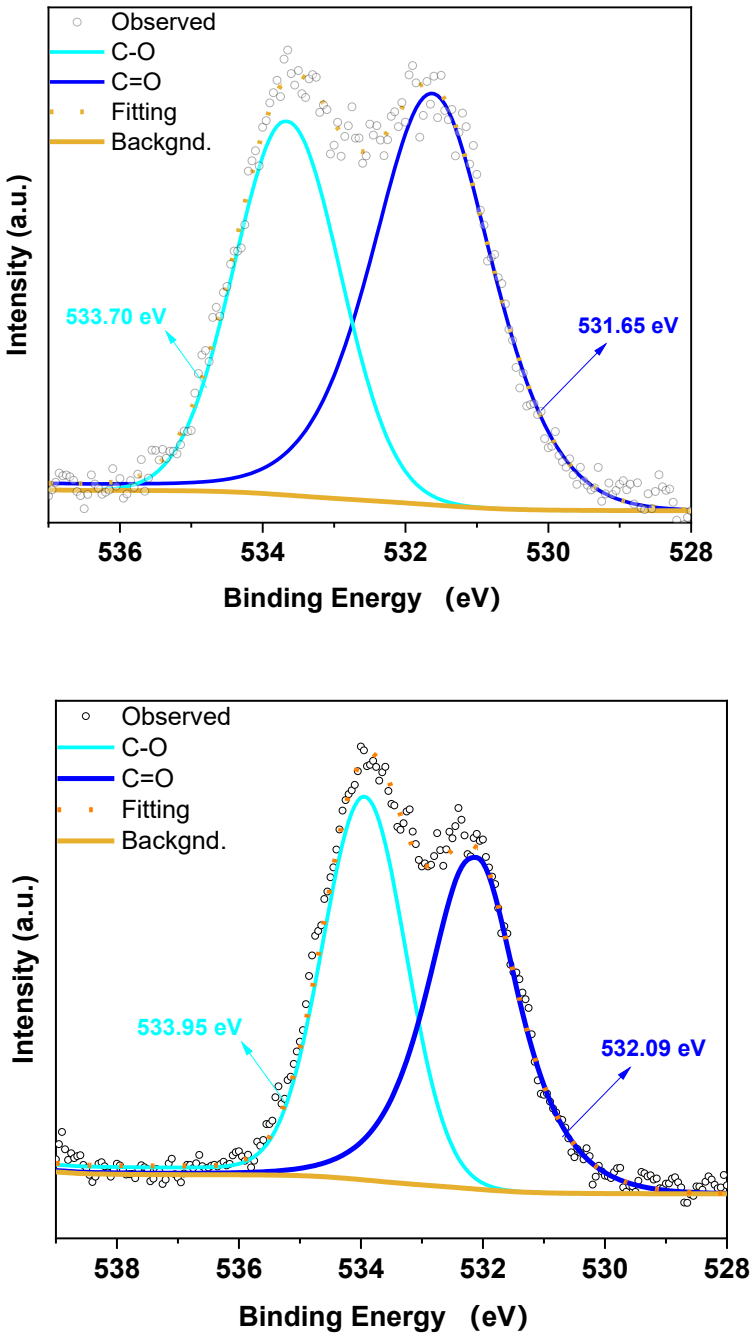

Fig. S25: C 1s XPS spectrum of **IPM-1** before (up) and after (down) iodine adsorption in gas phase.

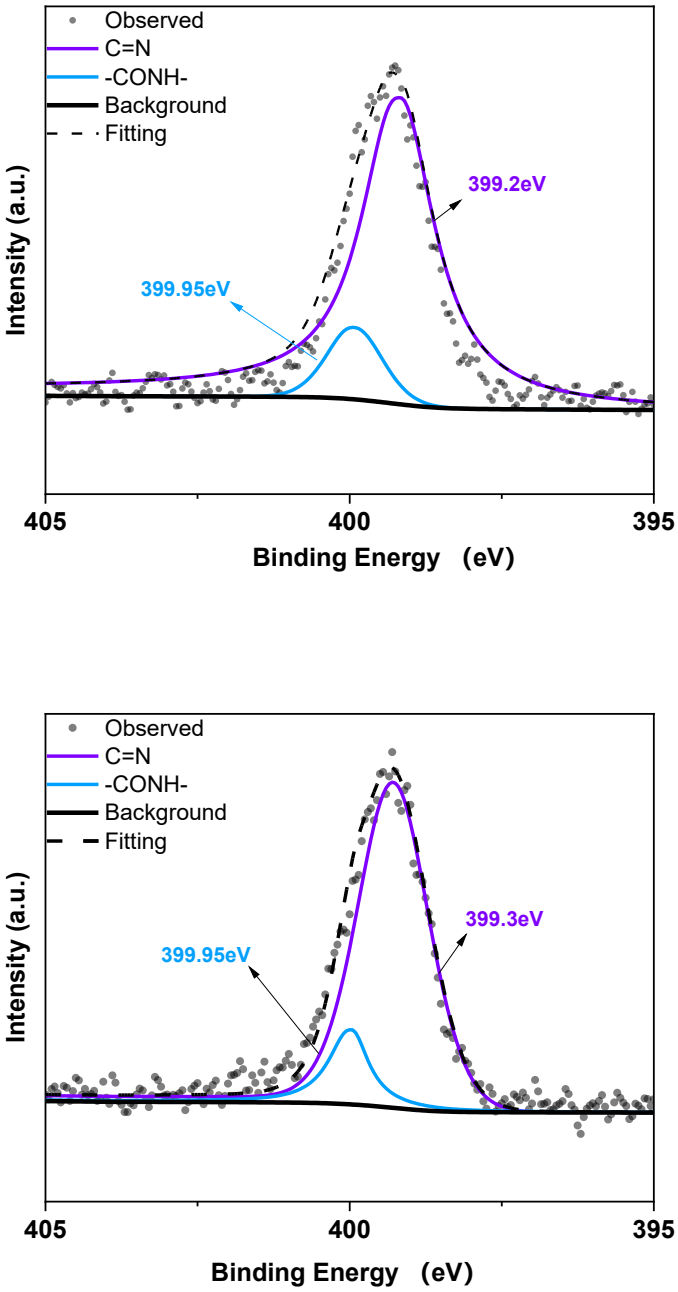

Fig. S26: N 1s XPS spectrum of **IPM-1** before (up) and after (down) iodine adsorption in gas phase.

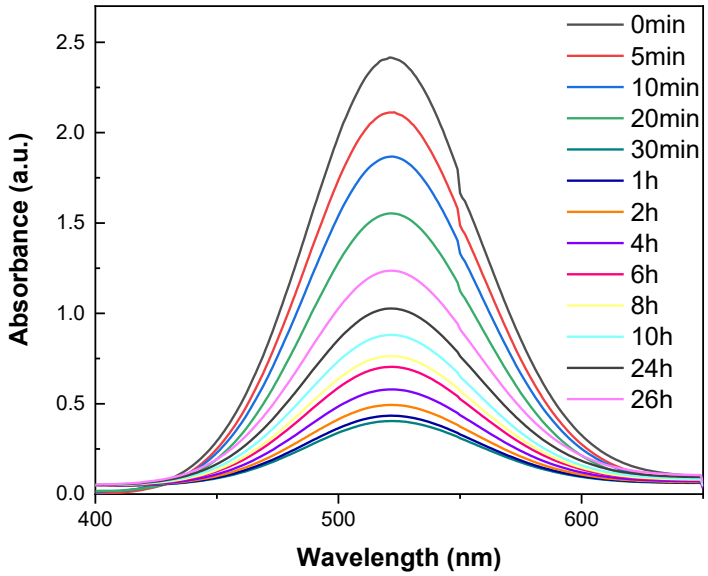

Fig. S27: The UV-Vis spectra show that **IPM-1** extracts I_2 from hexane over time.

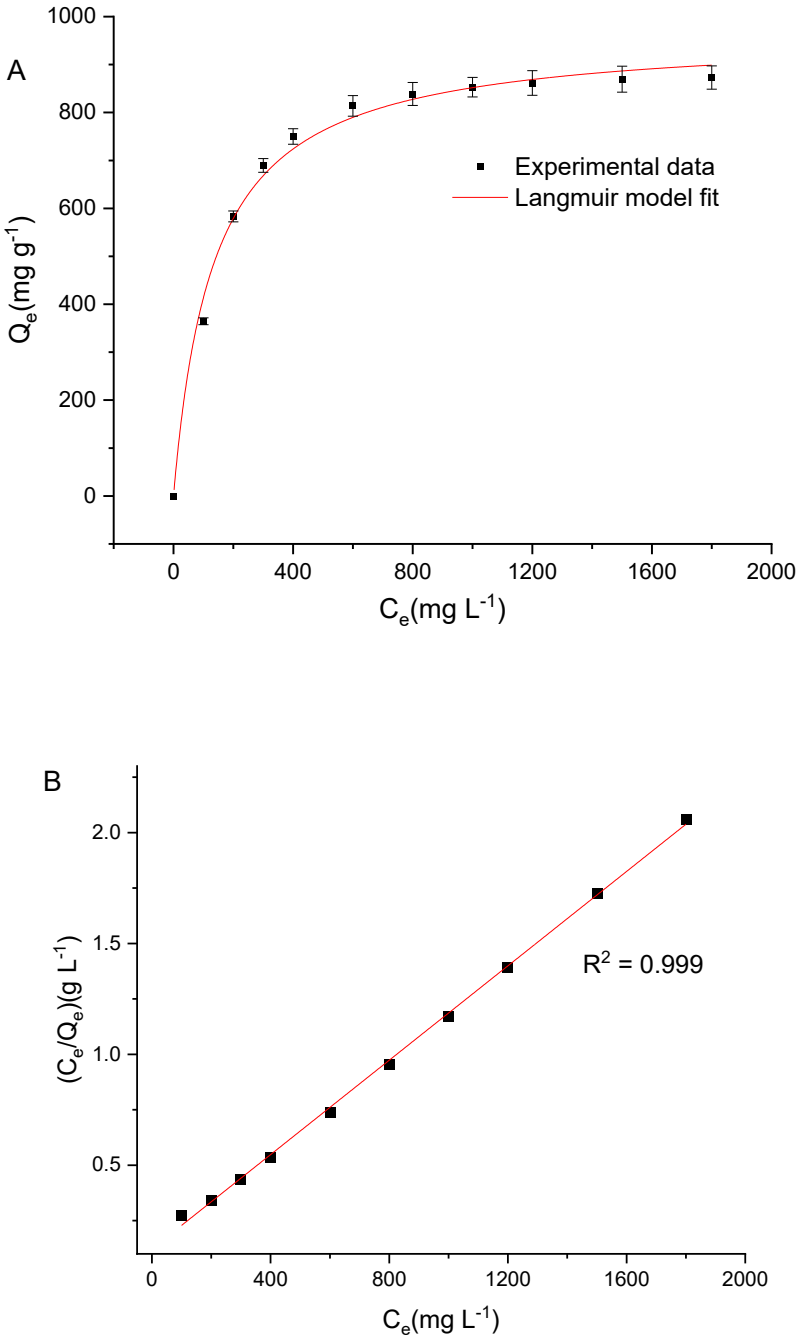

Fig. S28: Liquid-phase iodine uptake–time profile of **IPM-1** fitted with the Langmuir model.(A) Fitting curve based on the Langmuir model; (B) Corresponding fitting result with a determination coefficient $R^2 = 0.999$.

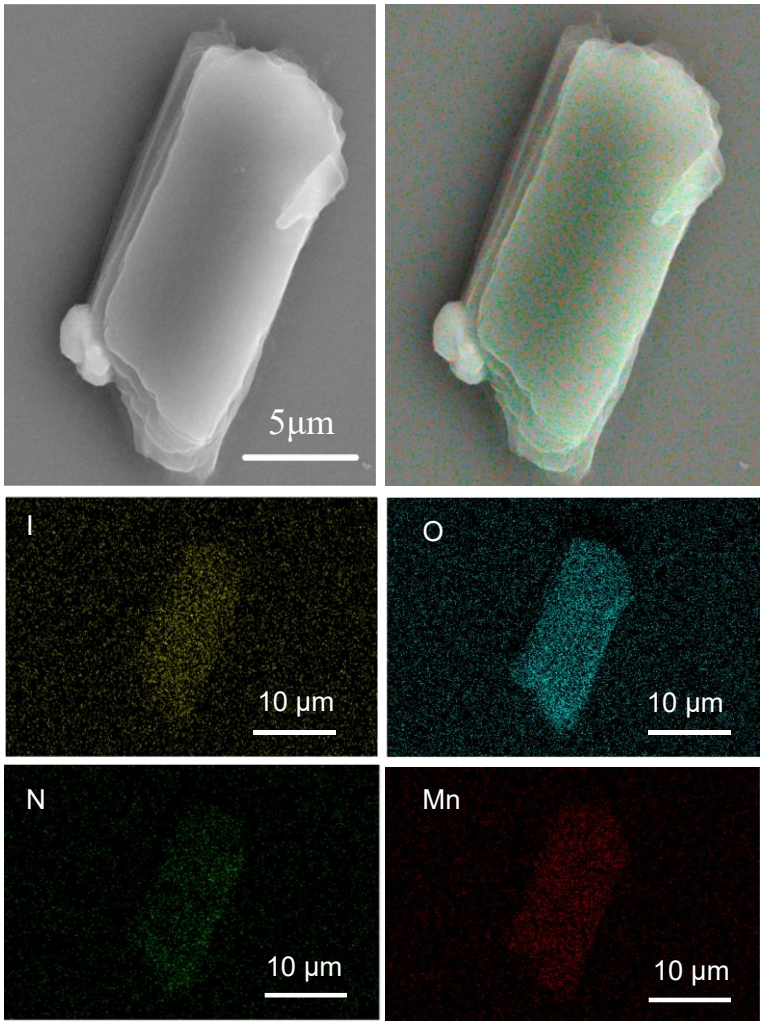

Fig. S29: SEM and EDS mapping images of **IPM-1** crystal co-crystallized with iodine in DMF.